



HAL
open science

Peptide Hydrogels Assembled from Enzyme-Adsorbed Mesoporous Silica Nanostructures for Thermoresponsive Doxorubicin Release

Bing Li, Miryam Criado-Gonzalez, Alexandre Adam, Joëlle Bizeau, Christophe Mélart, Alain Carvalho, Sylvie Bégin, Dominique Bégin, Loïc Jierry, Damien Mertz

► To cite this version:

Bing Li, Miryam Criado-Gonzalez, Alexandre Adam, Joëlle Bizeau, Christophe Mélart, et al.. Peptide Hydrogels Assembled from Enzyme-Adsorbed Mesoporous Silica Nanostructures for Thermoresponsive Doxorubicin Release. *ACS Applied Nano Materials*, 2022, 5 (1), pp.120-125. 10.1021/ac-sanm.1c03959 . hal-03872337

HAL Id: hal-03872337

<https://hal.science/hal-03872337v1>

Submitted on 25 Nov 2022

HAL is a multi-disciplinary open access archive for the deposit and dissemination of scientific research documents, whether they are published or not. The documents may come from teaching and research institutions in France or abroad, or from public or private research centers.

L'archive ouverte pluridisciplinaire **HAL**, est destinée au dépôt et à la diffusion de documents scientifiques de niveau recherche, publiés ou non, émanant des établissements d'enseignement et de recherche français ou étrangers, des laboratoires publics ou privés.

Peptide Hydrogels Assembled from Enzyme-Adsorbed Mesoporous Silica Nanostructures for Thermo-Responsive Doxorubicin Release

Bing Li^{1,2}, Miryam Criado-Gonzalez³, Alexandre Adam¹, Joëlle Bizeau¹, Christophe Mélar², Alain Carvalho³, Sylvie Bégin¹, Dominique Bégin², Loïc Jierry^{3,} and Damien Mertz^{1,*}.*

¹Institut de Physique et Chimie des Matériaux de Strasbourg (IPCMS), UMR-7504 CNRS-Université de Strasbourg, 23 rue du Lœss, BP 34 67034, Strasbourg Cedex 2, France

²Institut de Chimie et Procédés pour l'Energie, l'Environnement et la Santé (ICPEES), UMR-7515 CNRS-Université de Strasbourg, 25 rue Becquerel, 67087 Strasbourg, Cedex 2, France

³Université de Strasbourg, CNRS, Institut Charles Sadron (UPR22), 23 rue du Loess, 67034 Strasbourg Cedex 2, BP 84047, France.

KEYWORDS: peptide hydrogel, stellate mesoporous silica, thermo-responsive hydrogel, smart nanocomposite, drug delivery, enzyme-assisted self-assembly.

ABSTRACT. The development of nanocomposite supramolecular hydrogels which can be activated by local or external stimuli (pH, redox, enzyme, heat) is highly promising for various applications including implantable materials for anti-tumor or tissue engineering applications. Here, we show that large pore stellate mesoporous silica modified with isobutyramide grafts, allow >100% wt. loading of enzymes which ensures through the enzyme-assisted self-assembly

an easy, rapid and efficient way to design smart thermoresponsive nanocomposite supramolecular hydrogels. Typical temperature increase (42°C), which may be induced by hyperthermia anti-cancer treatments, leads to the controlled-release of doxorubicin encapsulated in the resulting peptide self-assembled material.

Introduction

Nowadays, the development of smart drug delivery polymer scaffolds able to respond to their biological environment (pH, redox, enzymes) or through external stimuli (light, magnetic field) has become a great challenge in the field of tissue engineering or implantable materials for anti-tumor applications¹⁻⁴. The chemical design of such advanced materials is faced to various issues: i) developing an easy-to implement approach of nanostructure's functionalization; ii) the need for a suitable design ensuring efficient drug release with eventually controlled doses (via burst or pulses) given that standard polymer scaffolds may load low amount of drugs iii) achieving suitable chemical and mechanical robustness. One way to solve such questions is to introduce biocompatible inorganic nanomaterials as building blocks within the polymer scaffolds given that they may provide mechanical reinforcement, and their surface would offer versatile surface chemistry to connect polymers. Hence, a suitable surface nano-engineering of the nanomaterials is needed to induce strong crosslinking within the organic/polymer architecture. Furthermore, it would allow to realize a controlled assembly of original polymers from the surface of the nanomaterials⁵⁻⁷ Additionally, the possibility of some responsive inorganic nanoparticles (NPs) like iron oxide ⁸⁻¹⁰, gold ^{11,12} or carbon nanotubes /graphene ^{13,14} to be part of the scaffold, is also a way to render the architecture sensitive to external stimuli, which essentially consist in converting light or radio-frequency magnetic field into local heating.

Hence, such approach would be a good mean to tune the materials properties and the drug release itself.

However, main challenges, especially for biomedical applications, are not only the design of controlled structures at the nano and macroscale but also the development of new properties such as chemical functionalization, mechanical stability and ability of drug release. Among possible NPs which can be used to achieve such nanocomposite scaffold design, mesoporous silica (MS) are relevant nanomaterials given their easy synthesis, versatile surface modification chemistry and their potential to treat various diseases¹⁵⁻¹⁷. Given their possibility to load various nanosize objects, such as large molecules, biopolymers, or even small dots NPs, large pore MS^{18,19} are particularly appealing as building blocks of the polymer scaffold or to induce polymer self-assembly from these NPs.

Besides, supramolecular polymerization of peptides is an interesting approach when enzymatically triggered. This process called enzyme-assisted self-assembly (EASA) is based on the enzymatic transformation of precursor peptides into a self-assembling one, leading to nanofibrous networks²⁰ which underpin a hydrogel²¹. Since the hydrogelation is induced by a biomacromolecule and working in physiological conditions, requiring no additional chemicals (initiators, toxic monomers, crosslinking reagents, etc), this approach is particularly suitable for biomedical applications.²² In addition, thanks to the enzyme location, the hydrogelation can be spatially controlled which has been recently illustrated for various applications²³⁻²⁹

In this letter, we address an efficient strategy to induce the hydrogelation process from large pore mesoporous silica NPs called stellate mesoporous silica (STMS). Such STMS NPs, loaded with enzymes, play the role of initiators of the self-assembly process and of cross-linking points for building efficiently the nanocomposite supramolecular hydrogel. Alkaline Phosphatase

(AP) and the precursor peptide Fmoc-FFpY (Fmoc: fluorenylmethyloxycarbonyl; F: phenylalanine; Y: tyrosine; p: phosphate group) are used as model systems (**Fig. 1**). An original strategy to immobilize AP on STMS is the use of isobutyramide (IBAM) grafts which allow to immobilize efficiently high amount of AP (100 wt% payload) which there after ensures rapid self-assembly process of peptide (1 hour). Furthermore, an antitumor drug model, doxorubicin (DOX) was successfully loaded along with the formation of homogenously distributed drug-loaded nanocomposite hydrogels (NC HGs). Mechanical reinforcements of the self-assembled peptide hydrogel induced by the AP-immobilized STMS, and also by the loaded drug itself, are shown in a rheology study. At last, the thermo-responsive behavior of such new designed NC HGs was demonstrated highlighting the potential of thermal release of DOX from such architectures.

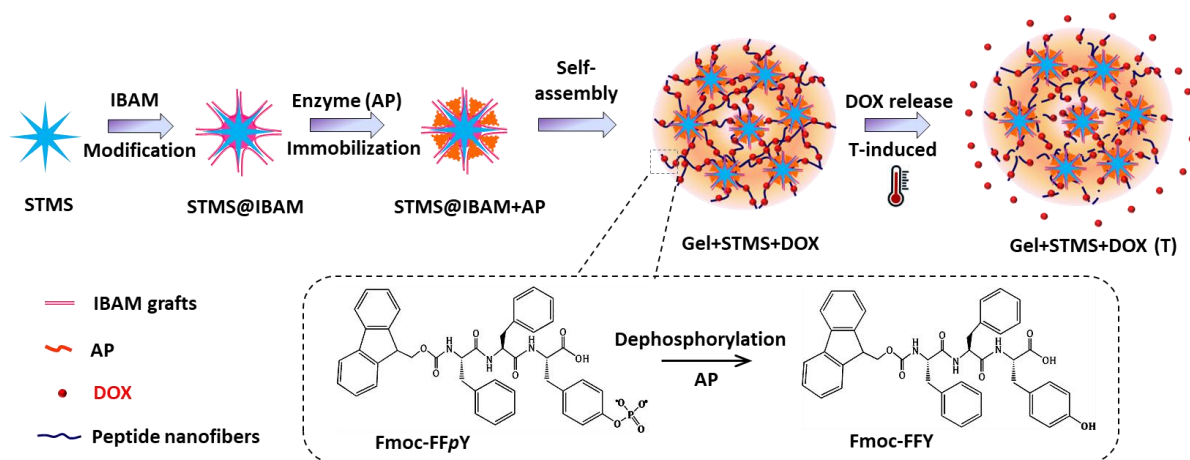


Figure.1 Scheme of the strategy used to design nanocomposite supramolecular peptide hydrogels generated from AP-immobilized STMS and its thermally-induced DOX release.

Results and Discussion

The first step of this work was to graft IBAM groups at the surface of STMS NPs and characterize the features of this grafted organic layer by transmission and scanning electron

microscopies (TEM-SEM), thermogravimetric analysis (TGA) and porosimetry. STMS nanoparticles were synthesized by using tetraethoxysilane (TEOS) as a silica precursor and cetyltrimethylammonium, tosylate (CTATos) as a structure-directing agent as reported in previous studies.^{19,30} TEM and SEM were used to characterize the structures of synthesized STMS particles, as shown in **Fig.S1**. It can be clearly observed from the TEM/SEM images that the STMS NPs are highly monodisperse showing a homogenous radial stellate mesoporous structure with an average size of 90 ± 7 nm. The SEM image displays porous spherical particles (**Fig.S1 B**). Especially, the open large pore channels of STMS are revealed both by TEM and SEM images. The nitrogen adsorption-desorption isotherms and the corresponding pore size distribution of STMS are shown in **Fig.S2 A**. According to the Brunauer-Emmett-Teller (BET) analysis, a BET surface area of $393\text{ m}^2/\text{g}$ associated with a pore volume of $1.06\text{ cm}^3/\text{g}$ was obtained. The pore size distribution calculated with the Barrett-Joyner-Halenda (BJH) model, indicates that STMS exhibits an average mesopore size *ca.* 11.2 nm (**Fig.S2 A**, inset). A detailed pore structure analysis of such STMS NPs was performed in a recent work.³⁰ Results indicated that in addition to the mesoporosity observed here (*ca.* 10 nm), there is also an important microporosity contribution observed with pore diameter below 0.5 nm. Then, STMS was modified with IBAM grafts as reported previously where the first step is a silanization with aminopropyltriethoxysilane (APTS), introducing amine groups, and a second step is their chemical transformation in isobutyramide (IBAM) moieties. BET analysis (**Fig.S2 B**) revealed a reduction of the surface area from 393 to $110\text{ m}^2/\text{g}$ and pore volume from 1.06 to $0.45\text{ cm}^3/\text{g}$. This is confirmed also by the BJH model which shows mesopore size reduction from 11.2 to 7.6 nm. All the data are summarized in **Table 1**.

Table 1. Textural parameters of STMS and STMS@IBAM

Sample	BET surface area (m ² /g)	Pore volume (cm ³ /g)	Mesopore size (nm)
STMS	393	1.06	11.2
STMS@IBAM	110	0.45	7.6

TGA was used to follow the successful grafting of APTS and IBAM. TGA curves depicting thermal decomposition of STMS, STMS@APTS and STMS@IBAM are showed in **Fig.S3**. In the case of bare STMS, the TGA curve shows that there is a negligible weight loss below 200 °C, which corresponds to the evaporation of physically adsorbed water. The greater weight loss on STMS@APTS and STMS@IBAM curves occurs in the range of 250-400 °C and is due to the removal of organic moieties from the composite. Using STMS as a baseline, the amount of grafting APTS and IBAM groups were estimated to 11.9 wt% and *ca.* 13.2 wt% of STMS, respectively. This allows us determining the graft density of APTS and IBAM groups on the silica surface to 3.3 and 2.6 per nm², respectively.

Then, the loading of AP enzyme, through physical adsorption, was investigated on STMS@IBAM NPs and compared to bare STMS NPs. The AP loading was evaluated by labeling AP with fluorescein isothiocyanate FITC (exc. 490/ em. 520 nm) and by using a spectrofluorimetry calibration curve: Intensity = f([AP^{FITC}]) (**Fig.S4**). This method allows the dosage of the remaining AP^{FITC} in supernatant and thus adsorbed on the NPs. **Fig.2 A** shows the enzyme immobilization capacities *q* (mg of AP adsorbed per mg of composite, black curves) and loading efficiencies (in %, blue curves) on STMS and STMS@IBAM, as a function of the initial enzyme concentration. Results show that the amount AP adsorbed on IBAM is linearly increasing while the one on bare NPs reach a plateau. At 4 mg/mL in AP, *q*(STMS@IBAM) reach *ca.* 1 mg AP/mg STMS while *q*(bare STMS) is close to 0.05 mg AP/mg STMS. [AP] was even increased to obtain the saturation plateau which was estimated at *ca.* 4 mg AP/mg STMS

when [AP] reach ca. 22 mg/mL (**Fig.S5**). TGA profiles (run in air from 25 to 800°C, 10°C/min) of STMS@IBAM loaded with AP^{FITC} in the range of [AP] = 0.5-25 mg/ml (**Fig.S6**) confirmed the huge amount of loaded enzymes found by spectrofluorimetry. The photographs of the STMS NPs show that with the increase of AP^{FITC} adsorbed, the composites become more and more colored in yellow (**Fig.S7**). Furthermore, Zeta potential (ZP) measurements achieved step by step confirmed the charge reversals after IBAM grafting and AP loading (100 wt%) (**Fig.S8**).

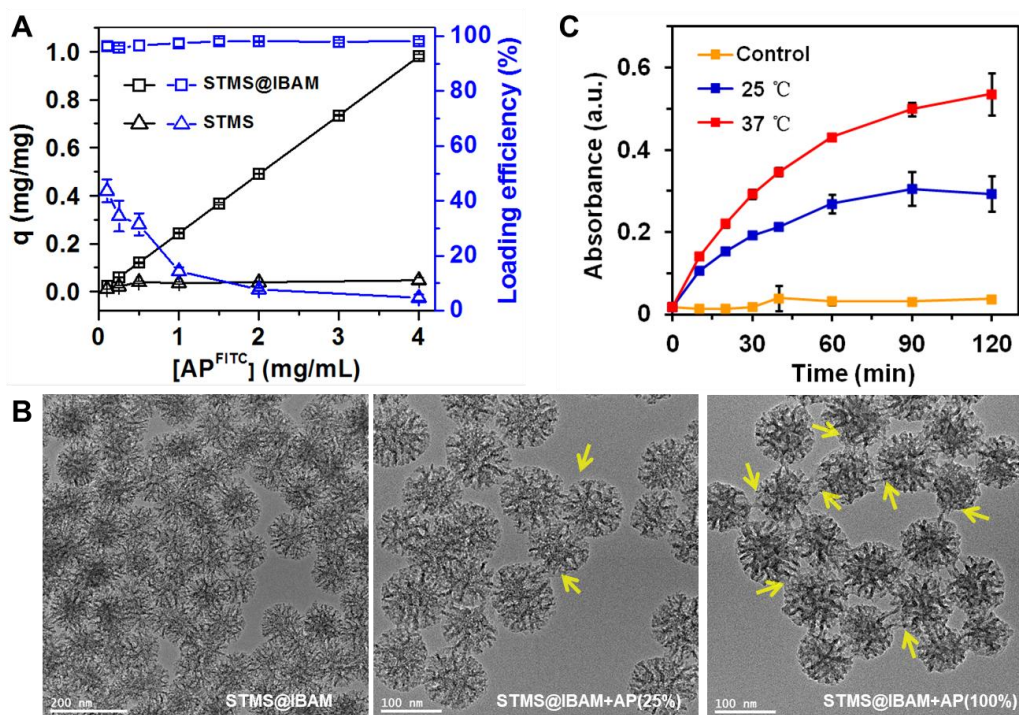


Figure 2. (A) Enzyme immobilization capacity q (mg of AP adsorbed per mg of composite) and loading efficiency (in %) on STMS and STMS@IBAM, as a function of the initial enzyme concentration. (B) Panel of TEM images of STMS@IBAM, STMS@IBAM (25 wt% AP) and STMS@IBAM (100 wt% AP). Yellow arrows indicate the sticky nature of the enzymes between the STMS NPs as observed through TEM. (C) Biocatalytic study displaying the absorbance of pNP at 25 and 37°C as a function of time, converted from 2 mL of pNPP (0.05 mg/mL) in the presence of 20 μ g of STMS@IBAM+AP (100 wt%). Control: 2 mL of pNPP (0.05 mg/mL) in

the presence of 20 μg STMS at 25 $^{\circ}\text{C}$. The absorbance was measured at $\lambda=405$ nm by UV visible spectrophotometry.

STMS@IBAM+AP nanocomposites were then imaged by TEM (**Fig.2 B**). Due to the presence of AP, dense and sticky organic matrix links were observed on the surface of STMS NPs which become more apparent with AP loading from 25 wt% to 100 wt%. The yellow arrows highlight that the adsorbed AP acts like “glue” to connect the nearby NPs. The size distribution and colloidal stability of STMS@IBAM+AP systems with different amounts of AP were measured by dynamic light scattering (DLS) in water at pH 6.5, as shown in **Fig.S9**. The DLS results show a monomodal dispersion of the IBAM-modified STMS with a hydrodynamic diameter determined at 164 nm (from TEM, the mean size of STMS is ca. 90 nm). Meanwhile, the hydrodynamic diameter of the NPs increased from 250 nm up to several microns with the amount of immobilized AP from 25 to 200 wt%, which is explained by the enhanced AP interconnection among the NPs.

At last, the biocatalytic activity of STMS@IBAM+AP (100 wt%) was evaluated by incubating the enzyme-coated NPs with a chromogenic substrate: p-nitrophenyl phosphate (pNPP) which is converted in a yellow colored product paranitrophenol (pNP), spectrophotometrically measured at $\lambda=405$ nm. Absorbance curves in **Fig.2 C** show thus the pNP product formation at 25 and 37 $^{\circ}\text{C}$ as a function of time, converted from 2 mL of pNPP in the presence of 20 μg of STMS@IBAM+AP (100 wt%). These curves show that the enzymatic activity (slope) is higher at 37 $^{\circ}\text{C}$ vs 25 $^{\circ}\text{C}$, as expected, the maximum activity being reported at 40 $^{\circ}\text{C}$ for this enzyme. No substrate conversion into product was observed in the absence of AP (control, STMS only). Photographs of the AP-immobilized STMS catalyzing the hydrolysis of pNPP to the yellow product pPN are showed in **Fig.S10**. These results reveal that the

immobilized AP maintain an efficient biocatalytic activity at the studied conditions. Such biocatalytic activity plays a key role in the synthesis of self-assembled supramolecular nanocomposite hydrogels.

In a next part, the formation of supramolecular Fmoc-FFY peptide hydrogel³¹ obtained by the dephosphorylation of Fmoc-FF p Y enzymatically catalyzed by the AP-coated STMS NPs was investigated. (Scheme, **Fig. 1**). Nanocomposites peptide HGs were thus formed through one pot synthesis by simply mixing the Fmoc-FF p Y peptides solution with the STMS@IBAM+AP (100 wt%) NPs in NaHCO₃ buffer. Resulting NC HGs display a uniform translucent color. (**Fig.3.A**, gel + STMS). The possibility of loading such hydrogels with DOX used as a model drug was also assessed. The use of hydrogels as drug reservoirs is not only promising for anticancer applications³² but also for other diseases such as chronic bladder diseases.³³ Hence, a full DOX loading was simply achieved by adding DOX aqueous solution to the previous one pot gel synthesis, resulting in the formation of a homogenous red-colored NC HG (**Fig.3.A**, gel + STMS+DOX). Typical Cryo-SEM images taken from Gel+STMS and STMS free hydrogel, prepared by using the free enzyme in same amount that the AP-coated on STMS were obtained. Dark gray individual STMS NPs can be easily observed from the Gel+STMS sample (**Fig.3 B**). The uniform and interweaved long peptide nanofibers are distributed around the AP-immobilized STMS NPs, suggesting that they are located at the nodes of the hydrogel network. Indeed, free STMS NPs meaning not included in the fibrous network, are not observed. For comparison, a typical cryo-SEM image in **Fig.S11** shows that the enzymatic dephosphorylation of Fmoc-FF p Y from free AP will also lead to the formation of Fmoc-FFY nanofibrillary structure. Noteworthy, in the presence of the AP-immobilized STMS composites, peptide nanofibers are guided by the immobilized AP generated from the surface of STMS. The NPs here play the role of cross-

linking points within the nanofibrous hydrogel network, which has the potential to enhance the mechanical properties of the hydrogel network.

The mechanical properties were determined by dynamic oscillatory rheology providing information about storage (G') and loss (G'') moduli of studied NC HGs (see **Fig. S12** for detailed study). At a frequency of 1 Hz and a strain of 1% (**Fig. 3.C**), storage modulus G' of the bare gel (Gel, formed by free AP) was measured at 9.5 ± 2.5 Pa while a significant increased value of 43.9 ± 2.7 Pa was obtained with the NC HG formed from AP-immobilized STMS in (Gel+STMS). This can be explained by the fact that AP-immobilized STMS act as crosslinking points of the peptide nanofibers network, and result in increased shear stiffness. Interestingly, the increase in elastic modulus was even higher when DOX was introduced, reaching a value of 72.7 ± 1.3 Pa. This observation suggests strongly the contribution of the antitumor agent in the hydrogel architecture which may reinforce weak interactions between peptide fibers and contribute to the macroscopic strengthening.

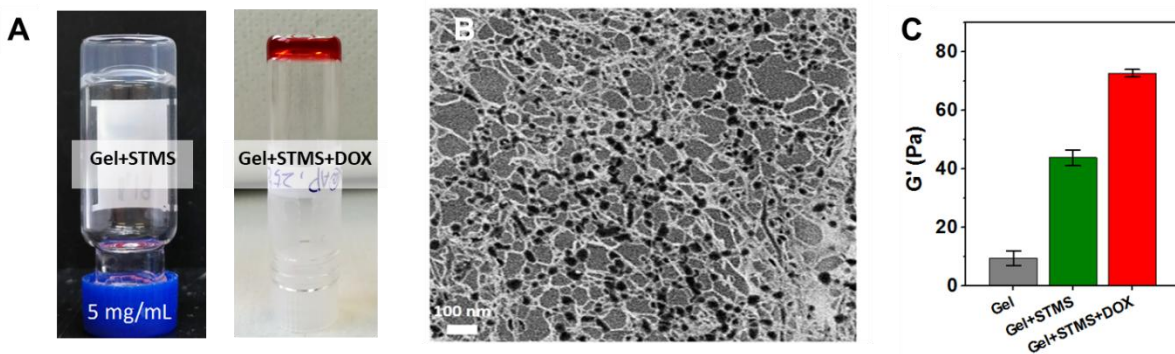


Figure 3. (A) Inverted tube tests of the self-assembled hydrogels without DOX (left) and with DOX (right). (B) Typical Cryo-SEM images taken from Gel+STMS. (C) Storage modulus (G') at 1 Hz, and 1% strain of bare hydrogel (Gel), Gel+STMS, Gel+STMS+DOX samples.

Next, with the aim to address the possibility of releasing DOX from these Gel+STMS+DOX through external stimuli, especially the temperature, the DOX loaded NC HGs were mixed with

1 mL of distilled water and then incubated at 25, 37, 42 °C for 24 h and at 42 and 50 °C for 48 h. DOX released was quantified by spectrophotometry using a calibration curve Absorbance vs [DOX] (**Fig.S13**). Hence, while the Gel+STMS+DOX stored at 25 °C for 24 h released in aqueous solution $3.0\pm 0.7\%$ of the initial loaded DOX, the NC HGs gels submitted to 37 °C and 42 °C released 7.7 ± 2.2 and $9.6\pm 1.4\%$ DOX in aqueous solution corresponding respectively 2.6 and 3.2 times more DOX released (**Fig. 4.A and B**). Furthermore, this thermally induced DOX release was even more accentuated by increasing the heating time (48h) and temperature (50°C) with 24.1 ± 1.5 and 28.9 ± 2.3 % DOX released respectively at 42 and 50 °C for 48 h. Control experiments at 25°C over 48h indicate at least two times lower release at $9.9\pm 4.7\%$. (**Fig.4 A and B**).

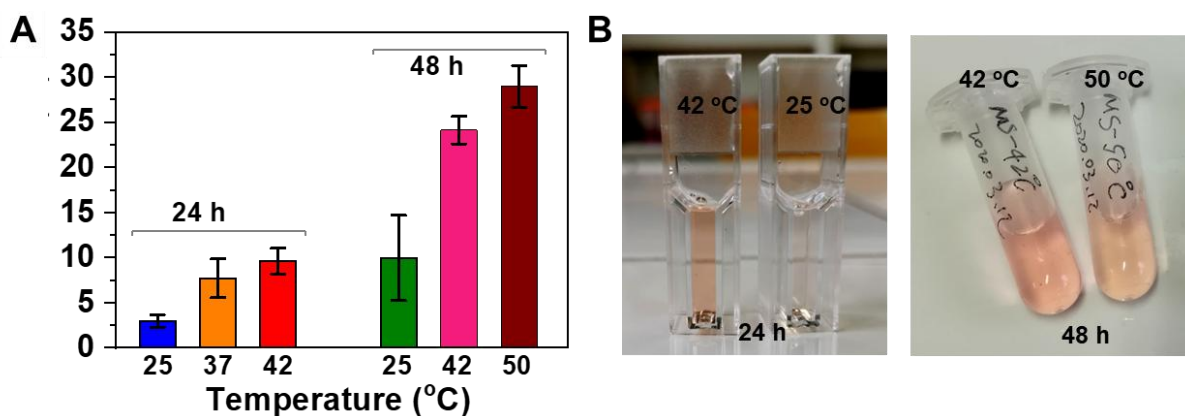


Figure 4. (A) DOX release from Gel+STMS+DOX at different temperature and time conditions. (B) Photographs showing DOX released into the aqueous solution at 25, 42 and 50 °C.

By looking at the structure of the NC HGs submitted to 42 and 50°C, they were found softer as compared to the gels at 25°C. By inverting the tubes to see gel formation, they tend to detach from the glass wall vials falling down and damaging in some pieces (**Fig. S14.A**). Rheology study on bare Gel and Gel+STMS+DOX confirmed the decrease of storage and loss moduli upon thermal treatment (see **Fig. S14.B**). The mechanical features of supramolecular hydrogels

contained-drugs prepared in bulk conditions have been recently shown behaving similarly once drug is loaded and released.³⁴ Nevertheless, it is noticed that the mechanical properties of STMS-containing gel after thermal treatment are still much higher than those of STMS-free gel.

Conclusion

In this work, a novel approach allowing the formation of NC HGs obtained by the self-assembly of peptides initiated from enzyme-capped STMS, was elaborated. Main results are:

- i) The immobilization of enzymes, with a very high loading capacity (>100% wt) is demonstrated within STMS thanks to the use of IBAM grafts as compared to bare surface.
- ii) As suggested by cryo-SEM observations and rheology, the NC HG material merely results from a peptide self-assembly network initiated from STMS NPs than from dispersed NPs within gel network. The DOX loading is shown to increase the elastic modulus, which suggests its involvement in the fiber network.
- iii) The formed NC HGs are shown to be thermo-responsive and are able to release DOX in aqueous solution upon thermal solicitation at 37, 42 and 50 °C as compared to ambient temperature.

Finally, the design of such thermo-responsive NC HGs open the way towards new antitumor scaffolds for hyperthermia induced-drug release for anti-cancer treatments.

Supporting Information. Materials and Methods. Figures S1. TEM and SEM images of STMS. S2. N₂ adsorption-desorption isotherms and S3. TGA of STMS, STMS@APTS and STMS@IBAM. S4. Calibration curve of AP^{FITC} in water. S5. Enzyme immobilization capacity and loading efficiency. S6. TGA of STMS@IBAM+AP^{FITC} with different amount of AP^{FITC} immobilization. S7. Photographs of STMS+AP^{FITC}, STMS@IBAM+AP^{FITC} with different

amount of AP^{FITC} immobilized. S8. Zeta potential and S9. DLS size distribution of STMS@IBAM and STMS@IBAM+AP in water (pH=6.5). S10. Photographs showing pNPP hydrolysis into yellow product pNP. S11. A typical Cryo-SEM image taken from supramolecular hydrogel prepared from free AP. S12. Storage and loss moduli of bare hydrogel (Gel), Gel+STMS, Gel+STMS+DOX. S13. Calibration curve of DOX in water by UV-visible spectrophotometry. S14. Photographs of hydrogels after the temperature treatments and rheology study.

AUTHOR INFORMATION

Corresponding Author

* Correspondence should be addressed to damien.mertz@ipcms.unistra.fr and loic.jierry@ics-cnrs.unistra.fr

Author Contributions

The manuscript was written through contributions of all authors. All authors have given approval to the final version of the manuscript.

ACKNOWLEDGMENT

D.M. acknowledges the Materials Institute Carnot Alsace (project ProtRemote) and the Agence Nationale de la Recherche (grant ANR-19-CE09-0004—Corelmag) for financial supports. Bing LI thank the Chinese Scholarship Council (CSC) for the grant during her PhD at CNRS and the University of Strasbourg. The Institute Charles Sadron microscopy platform is acknowledged for cryo-SEM analysis. The spectroscopy and the transmission electronic microscopy platforms of the IPCMS are acknowledged for technical supports.

REFERENCES

- (1) Satarkar, N. S.; Biswal, D.; Hilt, J. Z. Hydrogel Nanocomposites: A Review of Applications as Remote Controlled Biomaterials. *Soft Matter* **2010**, *6* (11), 2364–2371.
- (2) Gaharwar, A. K.; Peppas, N. A.; Khademhosseini, A. Nanocomposite Hydrogels for Biomedical Applications. *Biotechnol. Bioeng.* **2014**, *111* (3), 441–453. <https://doi.org/10.1002/bit.25160>.
- (3) Merino, S.; Martín, C.; Kostarelos, K.; Prato, M.; Vázquez, E. Nanocomposite Hydrogels: 3D Polymer–Nanoparticle Synergies for On-Demand Drug Delivery. *ACS Nano* **2015**, *9* (5), 4686–4697. <https://doi.org/10.1021/acsnano.5b01433>.
- (4) Mertz, D.; Harlepp, S.; Goetz, J.; Bégin, D.; Schlatter, G.; Bégin-Colin, S.; Hébraud, A. Nanocomposite Polymer Scaffolds Responding under External Stimuli for Drug Delivery and Tissue Engineering Applications. *Advanced Therapeutics* **2020**, *3* (2), 1900143. <https://doi.org/10.1002/adtp.201900143>.
- (5) Oh, J. K.; Park, J. M. Iron Oxide-Based Superparamagnetic Polymeric Nanomaterials: Design, Preparation, and Biomedical Application. *Progress in Polymer Science* **2011**, *36* (1), 168–189. <https://doi.org/10.1016/j.progpolymsci.2010.08.005>.
- (6) Skardal, A.; Zhang, J.; McCoard, L.; Oottamasathien, S.; Prestwich, G. D. Dynamically Crosslinked Gold Nanoparticle–Hyaluronan Hydrogels. *Advanced Materials* **2010**, *22* (42), 4736–4740.
- (7) Gaharwar, A. K.; Patel, A.; Dolatshahi-Pirouz, A.; Zhang, H.; Rangarajan, K.; Iviglia, G.; Shin, S.-R.; Hussain, M. A.; Khademhosseini, A. Elastomeric Nanocomposite Scaffolds Made from Poly (Glycerol Sebacate) Chemically Crosslinked with Carbon Nanotubes. *Biomaterials science* **2015**, *3* (1), 46–58.
- (8) Blanco-Andujar, C.; Walter, A.; Cotin, G.; Bordeianu, C.; Mertz, D.; Felder-Flesch, D.; Bégin-Colin, S. Design of Iron Oxide-Based Nanoparticles for MRI and Magnetic Hyperthermia. *Nanomedicine* **2016**, *11* (14), 1889–1910.
- (9) Kolosnjaj-Tabi, J.; Di Corato, R.; Lartigue, L.; Marangon, I.; Guardia, P.; Silva, A. K.; Luciani, N.; Clément, O.; Flaud, P.; Singh, J. V. Heat-Generating Iron Oxide Nanocubes: Subtle “Destructurators” of the Tumoral Microenvironment. *ACS nano* **2014**, *8* (5), 4268–4283.
- (10) Perton, F.; Tasso, M.; Muñoz Medina, G. A.; Ménard, M.; Blanco-Andujar, C.; Portiansky, E.; van Raap, M. B. F.; Bégin, D.; Meyer, F.; Bégin-Colin, S.; Mertz, D. Fluorescent and Magnetic Stellate Mesoporous Silica for Bimodal Imaging and Magnetic Hyperthermia. *Applied Materials Today* **2019**, *16*, 301–314. <https://doi.org/10.1016/j.apmt.2019.06.006>.
- (11) Dreaden, E. C.; Alkilany, A. M.; Huang, X.; Murphy, C. J.; El-Sayed, M. A. The Golden Age: Gold Nanoparticles for Biomedicine. *Chem. Soc. Rev.* **2012**, *41* (7), 2740–2779. <https://doi.org/10.1039/C1CS15237H>.
- (12) Liu, X.-Y.; Cheng, F.; Liu, Y.; Li, W.-G.; Chen, Y.; Pan, H.; Liu, H.-J. Thermoresponsive Gold Nanoparticles with Adjustable Lower Critical Solution Temperature as Colorimetric Sensors for Temperature, PH and Salt Concentration. *Journal of Materials Chemistry* **2010**, *20* (2), 278–284.
- (13) Vacchi, I. A.; Ménard-Moyon, C.; Bianco, A. Chemical Functionalization of Graphene Family Members. *Physical Sciences Reviews* **2017**, *2* (1).
- (14) Li, B.; Harlepp, S.; Gensbittel, V.; Wells, C. J. R.; Bringel, O.; Goetz, J. G.; Bégin-Colin, S.; Tasso, M.; Bégin, D.; Mertz, D. Near Infra-Red Light Responsive Carbon Nanotubes@mesoporous Silica for Photothermia and Drug Delivery to Cancer Cells.

- (15) Vallet-Regí, M.; Colilla, M.; Izquierdo-Barba, I.; Manzano, M. Mesoporous Silica Nanoparticles for Drug Delivery: Current Insights. *Molecules* **2018**, *23* (1), 47. <https://doi.org/10.3390/molecules23010047>.
- (16) Zhao, W.; Wang, H.; Wang, H.; Han, Y.; Zheng, Z.; Liu, X.; Feng, B.; Zhang, H. Light-Responsive Dual-Functional Biodegradable Mesoporous Silica Nanoparticles with Drug Delivery and Lubrication Enhancement for the Treatment of Osteoarthritis. *Nanoscale* **2021**, *13* (13), 6394–6399. <https://doi.org/10.1039/D0NR08887K>.
- (17) Zhou, S.; Zhong, Q.; Wang, Y.; Hu, P.; Zhong, W.; Huang, C.-B.; Yu, Z.-Q.; Ding, C.-D.; Liu, H.; Fu, J. Chemically Engineered Mesoporous Silica Nanoparticles-Based Intelligent Delivery Systems for Theranostic Applications in Multiple Cancerous/Non-Cancerous Diseases. *Coordination Chemistry Reviews* **2022**, *452*, 214309. <https://doi.org/10.1016/j.ccr.2021.214309>.
- (18) Knežević, N. Ž.; Durand, J.-O. Large Pore Mesoporous Silica Nanomaterials for Application in Delivery of Biomolecules. *Nanoscale* **2015**, *7* (6), 2199–2209. <https://doi.org/10.1039/C4NR06114D>.
- (19) Zhang, K.; Xu, L.-L.; Jiang, J.-G.; Calin, N.; Lam, K.-F.; Zhang, S.-J.; Wu, H.-H.; Wu, G.-D.; Albela, B.; Bonneviot, L. Facile Large-Scale Synthesis of Monodisperse Mesoporous Silica Nanospheres with Tunable Pore Structure. *Journal of the American Chemical Society* **2013**, *135* (7), 2427–2430.
- (20) Stendahl, J. C.; Rao, M. S.; Guler, M. O.; Stupp, S. I. Intermolecular Forces in the Self-Assembly of Peptide Amphiphile Nanofibers. *Advanced Functional Materials* **2006**, *16* (4), 499–508. <https://doi.org/10.1002/adfm.200500161>.
- (21) Yang, Z.; Gu, H.; Fu, D.; Gao, P.; Lam, J. K.; Xu, B. Enzymatic Formation of Supramolecular Hydrogels. *Advanced Materials* **2004**, *16* (16), 1440–1444. <https://doi.org/10.1002/adma.200400340>.
- (22) Du, X.; Zhou, J.; Shi, J.; Xu, B. Supramolecular Hydrogelators and Hydrogels: From Soft Matter to Molecular Biomaterials. *Chem. Rev.* **2015**, *115* (24), 13165–13307. <https://doi.org/10.1021/acs.chemrev.5b00299>.
- (23) Williams, R. J.; Smith, A. M.; Collins, R.; Hodson, N.; Das, A. K.; Ulijn, R. V. Enzyme-Assisted Self-Assembly under Thermodynamic Control. *Nature Nanotech* **2009**, *4* (1), 19–24. <https://doi.org/10.1038/nnano.2008.378>.
- (24) Vigier-Carrière, C.; Boulmedais, F.; Schaaf, P.; Jierry, L. Surface-Assisted Self-Assembly Strategies Leading to Supramolecular Hydrogels. *Angewandte Chemie International Edition* **2018**, *57* (6), 1448–1456. <https://doi.org/10.1002/anie.201708629>.
- (25) Wu, C.; Hu, W.; Wei, Q.; Qiao, L.; Gao, Y.; Lv, Y.; Liu, M.; Li, C.; Wang, X.; Wang, Q. Controllable Growth of Core–Shell Nanogels via Esterase-Induced Self-Assembly of Peptides for Drug Delivery. *Journal of Biomedical Nanotechnology* **2018**, *14* (2), 354–361. <https://doi.org/10.1166/jbn.2018.2492>.
- (26) Conte, M. P.; Sahoo, J. K.; Abul-Haija, Y. M.; Lau, K. H. A.; Ulijn, R. V. Biocatalytic Self-Assembly on Magnetic Nanoparticles. *ACS Appl. Mater. Interfaces* **2018**, *10* (3), 3069–3075. <https://doi.org/10.1021/acsami.7b15456>.
- (27) Criado-Gonzalez, M.; Fores, J. R.; Carvalho, A.; Blanck, C.; Schmutz, M.; Kocgozlu, L.; Schaaf, P.; Jierry, L.; Boulmedais, F. Phase Separation in Supramolecular Hydrogels

- Based on Peptide Self-Assembly from Enzyme-Coated Nanoparticles. *Langmuir* **2019**, *35* (33), 10838–10845. <https://doi.org/10.1021/acs.langmuir.9b01420>.
- (28) Criado-Gonzalez, M.; Iqbal, M. H.; Carvalho, A.; Schmutz, M.; Jierry, L.; Schaaf, P.; Boulmedais, F. Surface Triggered Self-Assembly of Fmoc-Tripeptide as an Antibacterial Coating. *Frontiers in Bioengineering and Biotechnology* **2020**, *8*, 938. <https://doi.org/10.3389/fbioe.2020.00938>.
- (29) Rodon Fores, J.; Criado-Gonzalez, M.; Chaumont, A.; Carvalho, A.; Blanck, C.; Schmutz, M.; Serra, C. A.; Boulmedais, F.; Schaaf, P.; Jierry, L. Supported Catalytically Active Supramolecular Hydrogels for Continuous Flow Chemistry. *Angewandte Chemie* **2019**, *131* (52), 18993–18998. <https://doi.org/10.1002/ange.201909424>.
- (30) Adam, A.; Parkhomenko, K.; Duenas-Ramirez, P.; Nadal, C.; Cotin, G.; Zorn, P.-E.; Choquet, P.; Bégin-Colin, S.; Mertz, D. Orienting the Pore Morphology of Core-Shell Magnetic Mesoporous Silica with the Sol-Gel Temperature. Influence on MRI and Magnetic Hyperthermia Properties. *Molecules* **2021**, *26* (4), 971. <https://doi.org/10.3390/molecules26040971>.
- (31) Hai, Z.; Li, J.; Wu, J.; Xu, J.; Liang, G. Alkaline Phosphatase-Triggered Simultaneous Hydrogelation and Chemiluminescence. *J. Am. Chem. Soc.* **2017**, *139* (3), 1041–1044. <https://doi.org/10.1021/jacs.6b11041>.
- (32) Huang, X.; Ding, L.; Liu, X.; Tong, R.; Ding, J.; Qian, Z.; Cai, L.; Zhang, P.; Li, D. Regulation of Tumor Microenvironment for Pancreatic Cancer Therapy. *Biomaterials* **2021**, *270*, 120680. <https://doi.org/10.1016/j.biomaterials.2021.120680>.
- (33) Qiu, H.; Guo, H.; Li, D.; Hou, Y.; Kuang, T.; Ding, J. Intravesical Hydrogels as Drug Reservoirs. *Trends in Biotechnology* **2020**, *38* (6), 579–583. <https://doi.org/10.1016/j.tibtech.2019.12.012>.
- (34) Mei, L.; Xu, K.; Zhai, Z.; He, S.; Zhu, T.; Zhong, W. Doxorubicin-Reinforced Supramolecular Hydrogels of RGD-Derived Peptide Conjugates for PH-Responsive Drug Delivery. *Org. Biomol. Chem.* **2019**, *17* (15), 3853–3860. <https://doi.org/10.1039/C9OB00046A>.